

Octyl-Decorated Fréchet-Type Dendrons: A General Motif for Visualisation of Static and Dynamic Behaviour Using Scanning Tunnelling Microscopy?

Leo Merz,^[a] H.-J. Güntherodt,^[a] Lukas J. Scherer,^[b] Edwin C. Constable,^{*,[b]} Catherine E. Housecroft,^{*,[b]} Markus Neuburger,^[b] and B. A. Hermann^{*,[c]}

Abstract: A detailed STM study of monolayers of 3,5-bis[(3,5-bis(octyloxyphenyl)methoxy)benzaldehyde and 3,5-bis[(3,5-bis(octyloxyphenyl)methoxy)benzyl alcohol adsorbed on graphite is presented. Very highly resolved scanning tunnelling microscopy images are observed at room temperature in air allowing the analysis of the conformation of the adsorbed molecules.

These long-chain alkyl-decorated Fréchet-type dendrons are a powerful assembly motif and initially form a pattern based on trimeric units, assembled

into hexagonal host structures with a pseudo-unit cell of seven molecules, one of which remains highly mobile. Over time, the supramolecular ordering changes from a trimeric into a dimeric pattern. The chirality arising from the adsorption onto a surface of the dendrons is discussed.

Keywords: adsorption • conformational analysis • dendrimers • scanning probe microscopy • self-assembly

Introduction

Self-assembly is a well-established phenomenon in chemistry^[1] and is widely utilised for the construction of extended two- or three-dimensional structures.^[2] Phase interfaces (solid–solid, solid–liquid, solid–gas, liquid–liquid, liquid–gas) are particularly suitable for the assembly of two-dimensional systems. Although originally little more than a chemical curiosity, two-dimensional self-assembly is assuming a significant technological importance.^[3] The current drive for miniaturisation of devices commenced with so-called top-down approaches, in which an existing macroscopic technology is

optimised to ever smaller scales. As one approaches the nanoscale with nanometre and subnanometre-scaled devices, the top-down approach reaches its practical and theoretical limits, as it is based on bulk state theories. As sizes shrink, the ratio of surface area to volume increases and surface properties tend to dominate the system. For example, gold clusters and nanoparticles have properties which differ significantly from bulk, metallic gold.^[4,5] A potential alternative is the bottom-up approach in which molecular components are used for the assembly of nanoscaled devices. The potential advantages in terms both of reaching the ultimate nonsubatomic limits and of material economy are compelling reasons for investigating the bottom-up methodology.^[6] Fundamental questions relating to the building, addressing, and control of such molecular-based devices remain unanswered. However, self-assembly, using molecular recognition interactions between molecules or between molecules and substrates, is an attractive candidate for the construction of nanoscaled devices.^[7] If the interactions are sufficiently well understood and the molecular components sufficiently well designed, then the self-assembled structure can be spontaneously formed.^[8] Applications require control at the molecular level, although the properties of surface-bound individual molecules or of the ensemble may not parallel the properties of single molecules. In particular, properties are likely to be highly dependent upon imperfections arising from substrate structure, foreign molecules, or ambiguous self-assembly motifs.

[a] Dr. L. Merz, Prof. Dr. H.-J. Güntherodt
Institute of Physics, Klingelbergstrasse 82, 4056 Basel (Switzerland)

[b] Dipl.-Chem. L. J. Scherer, Prof. Dr. E. C. Constable,
Prof. Dr. C. E. Housecroft, M. Neuburger
Department of Chemistry, Spitalstrasse 51, 4056 Basel (Switzerland)
Fax: (+41)61-267-1005
E-mail: edwin.constable@unibas.ch
catherine.housecroft@unibas.ch

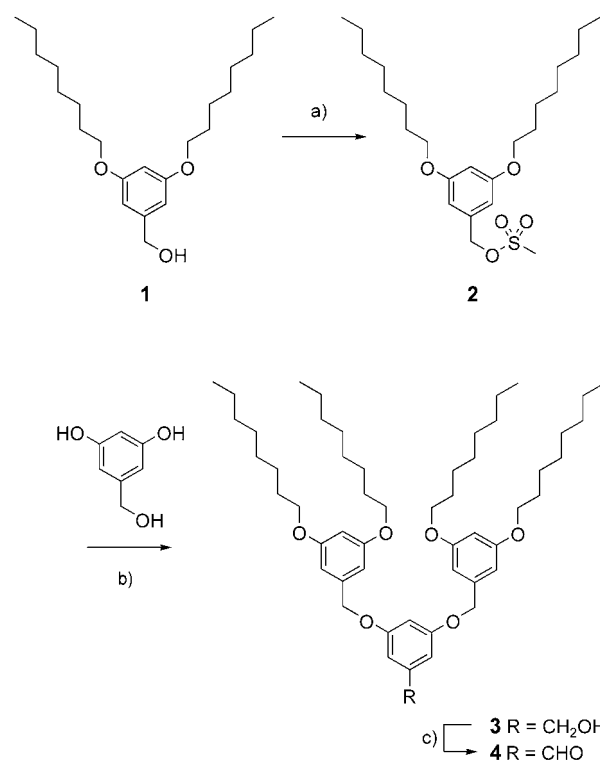
[c] Prof. Dr. B. A. Hermann
Walther-Meissner Institute and Faculty of Physics/Center for Nanoscience
LMU Munich, Walther-Meissner-Strasse 8, 85748 Garching (Germany)
Fax: (+49)89-289-14206
E-mail: b.hermann@cens.de

Scanning tunnelling microscopy (STM) is a powerful tool for obtaining structural and electronic data of surfaces and is particularly useful for characterising surfaces with non-periodic properties, observing small numbers of (or even individual) molecules, and for visualising irregularities, dynamic behaviour, or non-systematic defects.^[9,10] It is well established that STM may be used to monitor both the extent and detailed structure of surface-bound monolayers. In a few cases it has been possible not only to observe chemical species by STM, but also to move atoms^[11] or small molecules^[12] or to initiate and monitor chemical reactions of adsorbed molecules,^[13] although most studies of chemical reactions have been made at low temperatures on isolated molecules. Dynamic phase changes (two-dimensional Ostwald ripening) have been observed in adsorbed monolayers,^[14] as have reorganisation processes.^[15] The conformation of adsorbed molecules has a great effect on the properties of a monolayer^[16] and with scanning probe microscopes, it is possible to identify^[17–19] and change the conformation of molecules.^[20]

Early studies of molecular systems with STM were in ultra high vacuum^[10] but measurements under ambient conditions soon followed.^[21] In some cases, molecular and submolecular resolution STM images can be obtained at ambient temperature in air under conditions of chemical relevance.^[22–25]

A prerequisite for high resolution is a stable assembly that is not perturbed during the scanning process by the STM tip.^[22] High-resolution imaging allows both a direct or indirect analysis of the conformation of the adsorbed species,^[17,20,22,26–29] and the determination of the periodic properties of the ensemble.^[24,30] The technique can also be used to observe single events in real-space and -time.^[31]

We and others have shown that high-resolution images with submolecular resolution can be obtained of self-assembled monolayers of (*S,S*)-1,4-bis(dimethylamino)-2,3-dimethoxybutanes or 2,2'-bipyridines functionalised with octyl-decorated Fréchet dendrons and that in the latter case a detailed conformational analysis is possible.^[2,23] This leads us to the idea of suggesting the general use of long-chain alkyl-decorated Fréchet-type dendrons as visualisation markers for STM. The dendron functionalisation serves two purposes: firstly, the aromatic-rich structure and the alkyl chains combine to give a powerful self-assembly motif on graphite, and secondly, the high concentration of aromatic residues makes visualisation facile, as they act as STM markers. As a first step towards this proposition, we present a study of higher-generation Fréchet dendrimers 3,5-bis[3,5-bis(octyloxy)phenylmethoxy]benzyl alcohol (**3**) and 3,5-bis[3,5-bis(octyloxy)phenylmethoxy]benzaldehyde (**4**) (Scheme 1), the former having a known 3D crystal structure.^[32] Here we present studies of these achiral molecules and show that they form chiral domains upon adsorption on graphite. We also describe the STM observation of a metastable pattern, which rearranges to a stable one as a result of changing the supramolecular arrangement.



Scheme 1. Synthesis of alcohol **3** and aldehyde **4**. a) MesCl, NEt₃, CH₂Cl₂, -15 °C, 1 h; b) K₂CO₃, [18]crown-6, acetone, 60 °C, 48 h; c) pyridinium chlorochromate, molecular sieves 3 Å, CH₂Cl₂, room temperature, 4 h.

Results and Discussion

Synthesis and solid-state characterisation of compounds:

The octyl-decorated alcohol **3** has been reported by Seebach and co-workers^[32] and was the starting point for our investigations. An attractive feature of this compound was that a three-dimensional solid-state X-ray structure had been determined (CCDC Refcode WIRXOK). We used a modification of the literature method for the preparation of **3** using the mesylate **2** rather than the corresponding bromo derivative (Scheme 1). The mesylate **2** was prepared in high yield by the reaction of alcohol **1** with methanesulfonyl chloride and NEt₃ in dichloromethane at -15 °C. The crude mesylate **2** was then treated directly with 3,5-dihydroxybenzyl alcohol to give alcohol **3** in 76% yield (Scheme 1). The spectroscopic properties of **3** match those in the literature.^[3]

The reported solid-state structure of **3** was collected at 295 K and was refined to $R = 0.0872$, $wR^2 = 0.229$. Seebach mentions that no hydrogen bonding to the alcohol was observed. There was disorder present in the structure, with the alcohol oxygen disordered over two sites with C–O distances of 1.219 and 1.094 Å. We have determined the structure of **3** at 123 K (Figure 1).

All cell dimensions were within 2.5% of those of the published structure and the structure was refined to final R and wR factors of 0.0485 and 0.0565 ($I > 3\sigma(I)$). The structure at 123 K closely resembles that at room temperature, with the

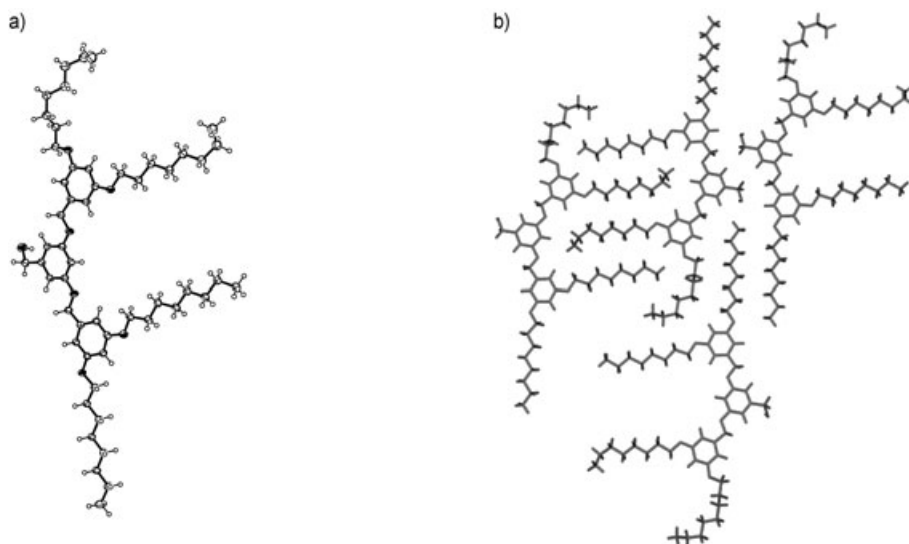


Figure 1. a) ORTEP plot (50% probability ellipsoids) of the solid state structure of **3** at 123 K. b) Part of a layer from the packing diagram of **3** showing the interdigitation of the alkyl chains.

exception that the alcohol is ordered with a C–O bond length of 1.417(3) Å. No intermolecular hydrogen bonding between the alcohol groups is observed.

We have also prepared the aldehyde **4**, which we initially thought might be an oxidation product in the single-crystal structure reported by Seebach et al. As the phenyl ether groups of the Fréchet-type dendrimers do not withstand treatment with MnO₂, alcohol **3** was oxidised with pyridinium chlorochromate and aldehyde **4** was formed in 91% yield. The aldehyde exhibited a characteristic C=O stretching mode at 1705 cm⁻¹ in its IR spectrum and in the ¹H NMR spectrum, the aldehyde CH was observed at $\delta = 9.89$ ppm.

Initial crystallographic studies of poor quality crystals of authentic **4** at 123 K revealed cell dimensions within 4% of those for **3**, and accordingly we can make no useful comment about the short C–O distances in the reported room-temperature structure of **3**.

Self-organised monolayers of 4 and 3: Monolayers of **4** and **3** were prepared at room temperature in air by placing a droplet of dilute solution (about 0.2 mm, *n*-pentane, *n*-hexane, *n*-decane, toluene, dichloromethane, acetone, or 1:1 dichloromethane/methanol) onto a freshly cleaved sample of highly oriented pyrolytic graphite (HOPG). After evaporation of the solvent, the samples were mounted in a commercial STM apparatus. Immediately after the approach of the STM tip, a periodic pattern was observed. STM images of organic molecules are often compared to representations of frontier orbitals.^[25,33] In a simplified treatment, a high conductivity results in a high intensity in the STM image and aromatic rings give particularly high contrasts. On the other hand, STM images of alkyl chains are usually of low intensity and low contrast. The images were recorded in constant-current mode in which the contrast is a measure of

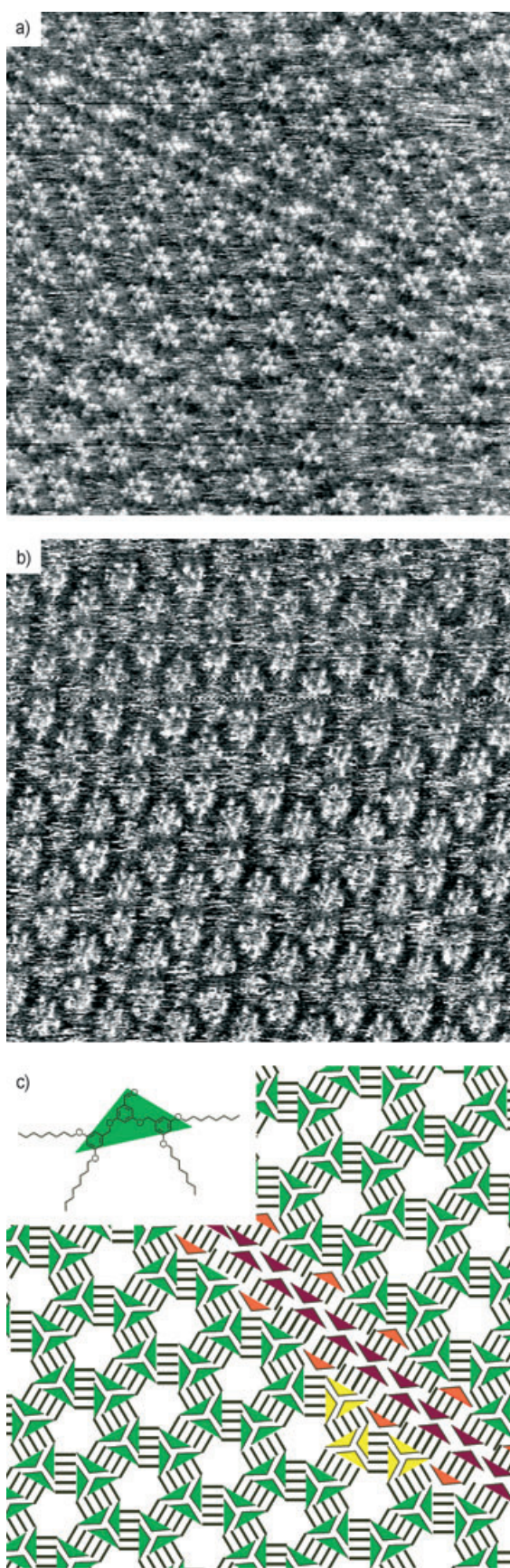
the height of the STM tip above the surface. The height of the tip above the surface is a function of the conductivity and of the physical topography of the sample. The observed 'flower pattern', which is shown in Figure 2, was seen for both **4** and **3**.

To maximise the two-dimensional crystallisation energy, the alkyl chains form interdigitated patterns with the alkyl chains of the neighbouring molecules, as is often observed for alkoxyated molecules adsorbed on surfaces,^[25,34,35] and the molecular arrangement is easily identified. The interdigitation of alkyl chains is also observed in the solid-state structure of **3** (Figure 1b).

Both **3** and **4** initially form monolayers. In each case, these comprise multiple domains with similar structures but different orientation.^[36] For each compound, three orientations of the domains were observed, reflecting the threefold symmetry resulting from the ABAB layer structure of α -graphite, in which every second atom in the A layer has an atom from the B layers directly underneath it. These domains consist dominantly of trimeric substructures as previously reported by the group of Bai for 3,5-bis[(3,5-bisdodecyloxyphenyl)methoxy]benzoic acid.^[37] However, we also comment upon an additional feature. In some domains of trimers, rows of embedded dimers were observed (Figure 2a and c). As expected, the rows of dimers show three orientations with respect to the surface. The STM images obtained were of sufficiently high resolution to allow a detailed analysis of the molecular conformation within the monolayers.

Analysis of the molecular and supramolecular conformation of the trimeric pattern: Images with very high resolution were obtained at room temperature in air. A further reduction of (random) noise by using an averaging procedure was helpful, but not mandatory to perform a conformational analysis, as we have reported previously.^[22] Figure 3 shows an averaged enlargement, and the proposed molecular arrangement of **4**.

The alcohol **3** was expected to form a six-membered central ring of hydrogen-bonded alcohol groups. The existence of the hydrogen bonds could only be inferred indirectly. The distances found between the aromatic moieties are consistent with an arrangement with a central ring of alcohol groups. Perhaps the existence of three hydrogen bonds is the reason for the increased stability of the layers of **3**. The layers of **4** are destroyed by scanning with about 50–100 pA tunnelling current, while the monolayers of **3** are stable up to about 100 pA. A higher current setpoint in STM also



means a shorter distance between tip and sample, and therefore more interaction between tip and sample (even though there is no contact). It can be concluded that the trimeric structure formed by **3** is slightly more stable than the structure formed by **4** under STM scanning conditions. Additionally, the monolayers of **3** are stable over larger periods of time than layers of the aldehyde. For months of measurements and reproducible data recording we thought that **3** does not undergo the transformation described below, because we only measured each sample for a couple of days; then we discovered that **3** also undergoes the conversion described below (see section about the conversion of the supramolecular arrangement). Often, STM images are compared to the frontier orbitals of the molecules, and a relationship between them can be found.^[25,33] However, images with the highest resolution should be compared to the frontier orbitals of the *adsorbed* species, or the frontier orbital interacting with the orbitals of the substrate, respectively. Such calculations would be a major undertaking. For small molecules, the STM image can be simulated by use of scattering theories, as has been done for molecules like benzene on graphite.^[38] Fisher and Blöchl calculated that the STM image of benzene strongly depends on the adsorption site and the applied potential. They predicted a three-fold symmetry for benzene on graphite (at certain lattice spaces), reflecting the three atoms that are seen with STM of each graphite hexagon.^[38] Our most highly resolved images of **4** indeed show three protrusions per phenyl ring, even for molecules much larger than benzene, as can be seen in Figure 3a. This high resolution allows a conformational analysis of the adsorbed molecules. We showed earlier^[22] that highly resolved STM images of adsorbed Fréchet dendrimers can be used to identify the conformation. Owing to the low contrast of the alkyl chains, only the conformation of the Fréchet-type part of the dendrons can be determined with certainty. Molecules **3** and **4** adopted the asymmetric conformation shown in Figure 3b and were found adsorbed on either face.

Chirality of the layers: Another reason for the interest in self-assembled monolayers is the breaking of symmetry that results from the interaction with the substrate on only one face.^[24,39] Both **4** and **3** are achiral molecules. They become prochiral when they are constrained to a planar conforma-

Figure 2. Two 40 × 40 nm STM images and a cartoon of the observed pattern. Bright features represent protrusions; dark features depressions. The *z* scale (height) of all shown images is approximately 0.2 nm (from black to white). a) A monolayer of **4** prepared from a hexane solution, forming trimers and a row of dimers (parameters: $I_t = 8$ pA, $U_{\text{bias}} = -700$ mV). b) A monolayer of **3**, prepared from a toluene solution (parameters: $I_t = 20$ pA, $U_{\text{bias}} = -600$ mV). c) A representation of the observed pattern observed for **4**, including a row of dimers (purple). The inset explains the schematic representation; the diagram is simplified and only four alkyl chains are shown for clarity. Aromatic moieties give a high contrast in STM, and aliphatics only a low contrast, owing to their low conductivity. See also Figure 4. The scanning parameters are listed in the Experimental Section.

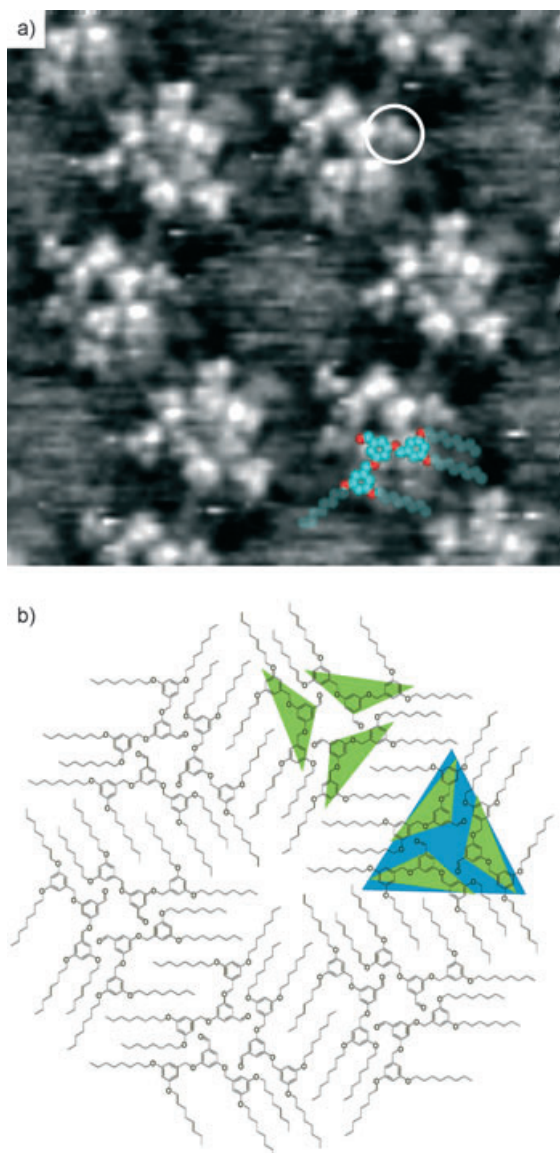


Figure 3. a) A 10×10 nm image ($I_t = 8$ pA, $U_{\text{bias}} = -700$ mV) of a monolayer of **4** prepared from a hexane solution, averaged over ten positions of a domain with counter-clockwise orientation with atomic resolution, showing three protrusions per phenyl ring (example marked with a circle). The conformation of the molecules is indicated with the overlaid molecular structure (C: green; O: red). The alkyl chains are drawn semi-transparent because they give little to no contrast in the STM images. b) The proposed molecular arrangement for **4**. Note that in image 3 a, it appears that poorly resolved alkyl chains can be seen.

tion. Figure 4 shows trimers of **4** which are mirror images. These trimers are prochiral. Upon adsorption onto a surface, the symmetry is reduced and the supramolecular arrangement becomes chiral, having a sense of direction as indicated with the circular arrows.

Because only the aromatic moieties give a high contrast in STM, the molecules can be represented in cartoon form as triangles, as shown in Figure 3b (green). These form trimers that again can be represented as triangles (blue). The trimers form hexagons and each presents a row of alkyl

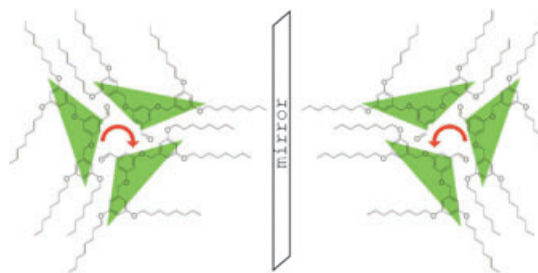


Figure 4. Mirror images of the same trimer of **4**. These prochiral trimers become chiral upon adsorption on a surface. The sense of orientation depends on the face onto which they adsorb to the surface.

chains to the neighbouring trimer. As a result, optimum interdigitation is achieved and the two-dimensional crystallisation energy is maximised.

The green triangles formed by the aromatic moieties of the molecules (Figure 4) do not point towards the centre of the trimers, but either to the left or to the right of it. The triangles formed by the trimers (Figure 5) do not point towards the centre of the hexagons. A hypothetical substrate-free monolayer of trimers would be correctly described as prochiral—adsorption on the graphite would differentiate the two prochiral faces and result in the formation of a chiral monolayer. Figure 5 shows both mirror images of the trimeric pattern. We call the orientation either clockwise (Figure 5a) or counter-clockwise (Figure 5b), depending on the arrangement of the trimers. Only homochiral domains of this trimeric pattern were observed. Both chiralities were found in equal proportions, but they were separated in different domains. This chiral, trimeric flower pattern was observed for both **3** and **4**.

The seventh molecule: At the centre of each hexagonal array of trimers of **3** or **4**, we observed an unresolved, noisy centre. Using the averaging procedure described in the experimental section, the ordered molecules become better resolved, but the noisy centre is smoothed out. The height of the centre in the raw data (Figure 2) is roughly the same as for the ordered molecules. In the averaged image (Figure 3), the height of the centre is less than the aromatic parts of the fixed molecules. This indicates random noise, which is generated by mobile molecules. Further proof that the random noise arises from the presence of *one* molecule confined to an area of roughly 2 nm^2 but remaining mobile is given below.

On very rare occasions, a hexagonal motif without a noisy centre could be observed for **3**. Such a vacancy, where the height of the bare graphite is seen,^[40] is shown in Figure 6, which further indicates that there is a mobile molecule in most noisy centres.

Similar phenomena were observed in X-ray analyses of trimesic acid (TMA) hydrogen-bonded structures that leave cavities filled with solvent molecules, which may retain a degree of mobility within a cavity.^[41]

Scanning tunnelling microscopy can resolve and distinguish static and dynamic molecules. The mobile molecule in

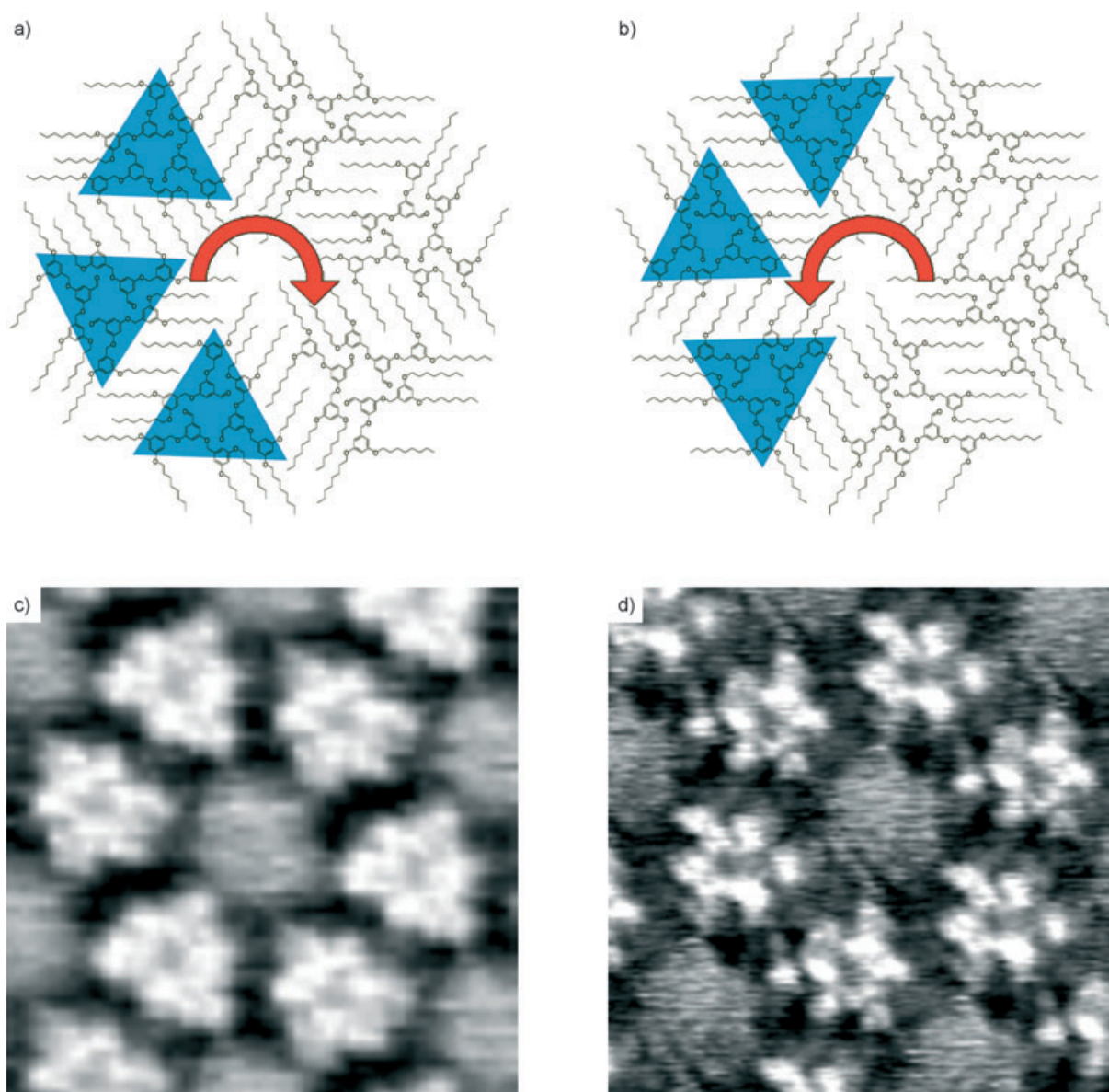


Figure 5. Both mirror images, clockwise (a) and (c) and counter-clockwise (b) and (d) of the trimeric pattern formed by **4**. STM images (c) and (d) are each 10×10 nm; (c) is averaged over 21 positions and (d) is averaged over 16 positions.

the centre of the hexagonal array simply has no unique “partner” with which to form an interdigitating pattern with its alkyl chains. At room temperature, the motion of the molecule is faster than the time scale of the STM measurements. Neglecting the randomness of the orientation of the central molecule, these ‘hexagonal’ patterns have a unit cell of *seven* molecules, comprising two trimers and one mobile molecule in the centre.

Rows of dimers: Embedded in the domains of trimers of adsorbed **3** or **4**, are single rows of dimers, as can be seen in Figure 2a and 2c. The space between the neighbouring half-hexagons (yellow) and a row of dimers (purple) is filled with single molecules (red) that form an interdigitating pattern of their alkane chains with those of the dimers. A sche-

matic representation of this pattern is shown in Figure 2c. These single molecules have less space available than the mobile molecules in the centre of a hexagon and, what seems more important, they have a “partner” available to allow interdigitation of the alkyl chains. One molecule of the row of dimers extends its alkyl chains towards this molecule, and the molecule is fixed in its location and can therefore be imaged with STM. These molecules present their aromatic region towards the half-hexagon, which is a further indication that no alkyl chains are extended towards the centre of the hexagons.

Delayed conversion of the supramolecular arrangement: The trimeric patterns observed for both **3** and **4** were not stable over time. After minutes to hours, a conversion into a

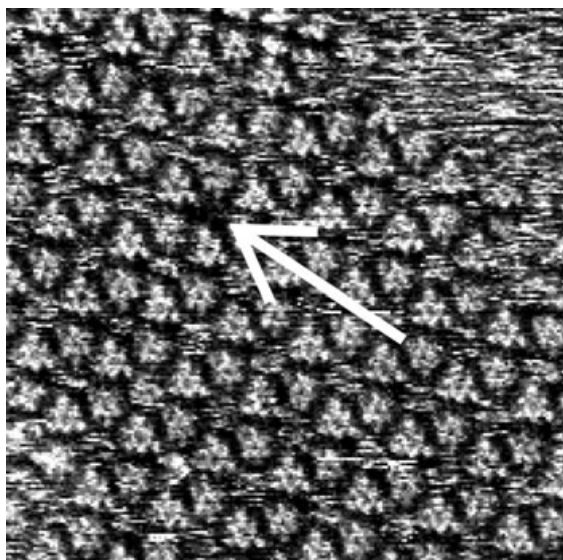


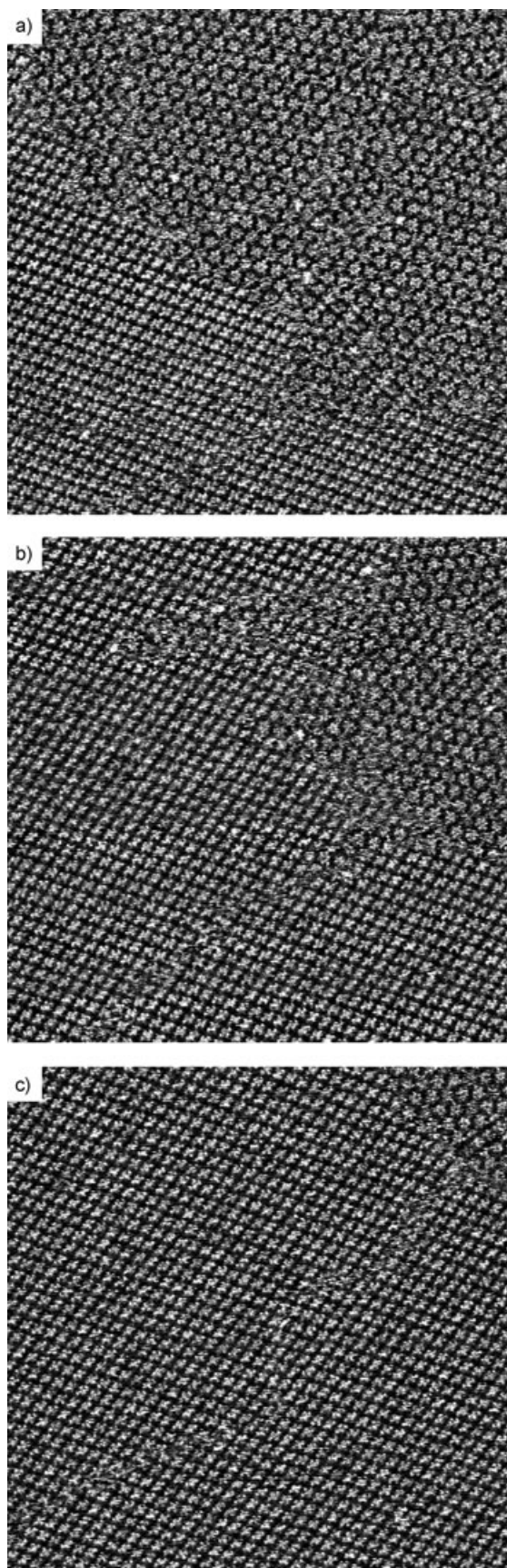
Figure 6. A rare 40×40 nm image ($I_t = 8$ pA, $U_{\text{bias}} = -700$ mV) of a vacancy in the trimeric pattern (marked with an arrow) for **3**. The monolayer was prepared from a hexane solution. On the top right of the image, the edge of the domain can be seen. The graphite there is covered with highly mobile molecules, leading to streaky noise. The vacancy inside the pattern shows the bare graphite.

different assembly started. This conversion could be followed in real time by STM measurements. While measuring the domains of trimers, a domain, consisting of dimers, appeared from outside of the observed window in the measurement and spread over all the observed area. The dimers formed a lamellar phase. One of the observed conversions is shown in Figure 7.

The newly formed pattern of dimers was stable over days, and no further conversion could be observed. The structural and conformational analysis of this new monolayer is given in the next section. The dimers also form a chiral pattern, because the two molecules do not face each other directly, but are closer together with a lateral offset. Figure 8 shows an example of the final dimeric pattern.

Both chiralities (offset to the right or offset to the left) were observed, separated in homochiral domains. The domains of dimers were of much larger size than those of the trimers. Again, the pattern was observed in the three equivalent orientations of the graphite surface. These lamellar regions were very well ordered and images of domains up to 400×400 nm were commonly observed. The software resolution (512×512 pixels) precluded the observation of molecular structure within larger windows and we can merely state

Figure 7. A sequence of 100×100 nm STM images for compound **4**, showing a conversion of the supramolecular arrangement (parameters: $I_t = 9$ pA, $U_{\text{bias}} = -700$ mV). a) A domain of dimers appears at the bottom left of the scan-window. At the top right of the image, several domains of trimers are seen. b) As the conversion continues, more and more of the trimers rearrange into dimers. c) The conversion is almost complete. The sample was prepared from hexane. Each image took about 6 min to record.



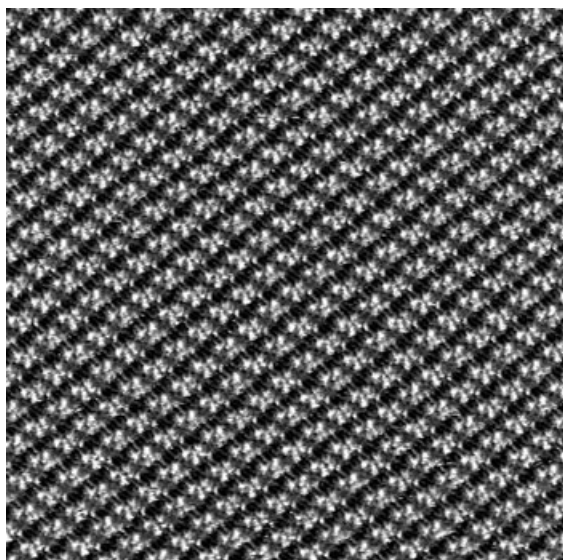


Figure 8. A 50×50 nm image of dimers of **4**, prepared from a hexane solution. Even the low contrast of the alkyl chains is recognisable, forming aliphatic and aromatic lamellae. Compound **3** shows identical lamellar phases after the conversion. (Parameters: $I_t = 8.5$ pA, $U_{\text{bias}} = -700$ mV.)

that individual domains were significantly greater than 160000 nm² without defects or vacancies. The structure of the dimeric domains differs from that of the rows of dimers observed in the original trimeric monolayers and *no* isolated dimeric rows were seen in the large dimeric domains. In rare cases, two domains were found with either an angle of 120° or a linear offset between them. By thermal annealing (70°C) of a freshly prepared trimeric sample, a structure with smaller domains consisting of dimers could be prepared. Under these thermal conditions, multiple domains of dimers were observed.

Conformational analysis of the dimeric pattern: As a result of the high resolution of dimeric domains, the conformation of the individual molecules forming the dimers could be assigned, as shown in Figure 9. In the dimeric arrangement, molecules of both **3** and **4** showed the asymmetric conformation shown in Figures 9 and 3b. The compounds potentially exhibit a high degree of conformational divergence, although the possibilities in conformational space are considerably reduced if we exclude the (unobserved) polymethylene chains from the discussion. The principal conformational freedom is then associated with the C-O-CH₂-C units. Somewhat surprisingly, a survey of all aromatic ethers in the Cambridge Crystallographic Data Base revealed a strong preference for the OCH₂C residue to lie in the plane of the attached aromatic ring.^[42] With an assumption of planarity, each ether unit can adopt a *syn* or an *anti* conformation (defined with respect to the C4 proton). A unique fit to the STM images is obtained with a *syn,anti* conformation at the central aromatic ring and *syn,syn* and *syn,anti* conformations at the outer rings. Detailed analysis of the conforma-

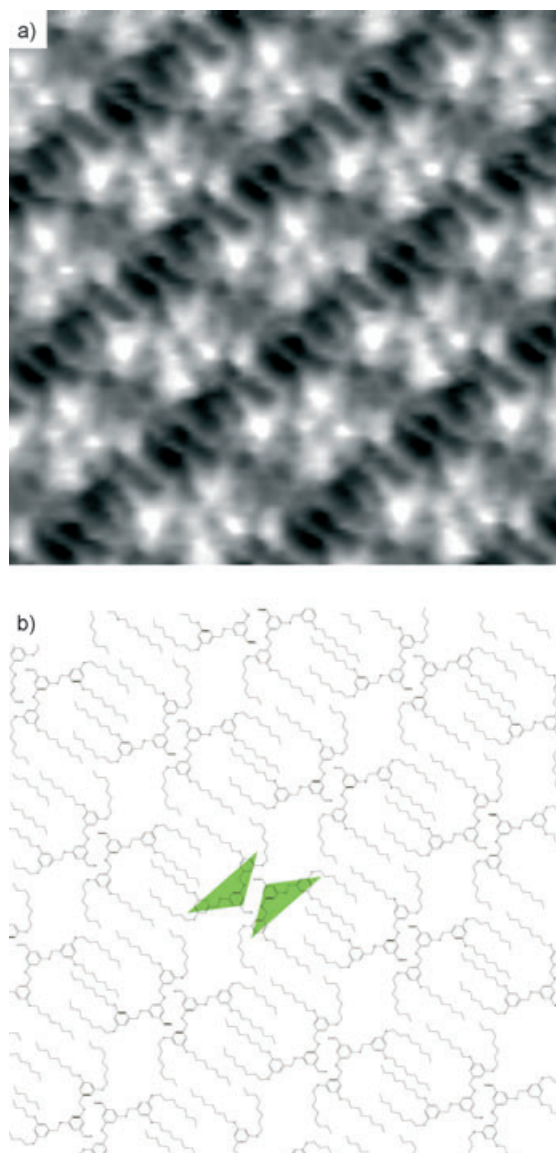


Figure 9. a) A 10×10 nm enlargement of the dimeric structure of **4** averaged over 14 positions. Even the lower contrast of the alkyl chains can be observed. The sample was prepared from a hexane solution. (Parameters: $I_t = 8.5$ pA, $U_{\text{bias}} = -700$ mV.) b) A molecular model of the proposed arrangement of molecules of **4**. The chirality or handedness can be clearly seen as an offset to the left or right with respect to the other molecule of the dimer.

tion of Fréchet-type dendrimers and their metal complexes will be given in a future publication.

Because of the observed spontaneous conversion of the trimeric to dimeric arrangements, the question of the nature of the mobile centre of the hexagons could be answered. The surface coverage was determined for both arrangements. Under the assumption that the number of molecules per unit area for a given domain remains constant, we calculated that exactly *one* molecule must form the mobile centre of the hexagons. The lamellar phase was observed to be stable over several days, and no further change was ob-

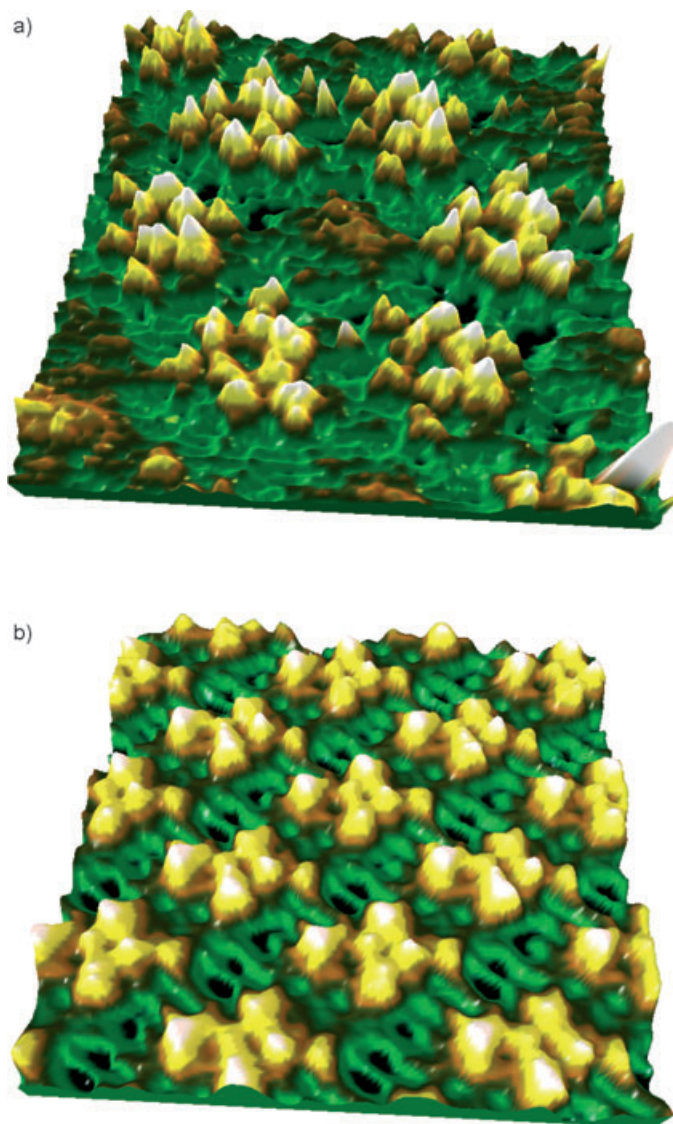


Figure 10. a, b) Two 10×10 nm 3D illustrations of the trimeric and dimeric patterns observed for compound **4**. The smooth central part of lower height in the centre of the averaged trimeric pattern can be seen (a). The samples were prepared from a hexane solution. The images are rendered in Pov-Ray 3.5 using the averaged three-dimensional data from the program SXM-shell.

served in any case. The next question to be addressed is what triggers the conversion of trimeric to dimeric monolayers and why the trimeric arrangement often appears metastable.

Trigger and driving forces for the trimer to dimer conversion:

There is no evidence that the rows of dimers found in the trimer phase initiate the trimer to dimer conversion. They have a different orientation on the graphite than the dimers of the lamellar pattern, and the embedded rows of dimers proved to be stable over observed times of minutes to days; they were even on occasion converted into the lamellar domain with a different orientation, as can be seen in

Figure 7. A few of the other obvious candidates for the initiation could be excluded as follows. The STM scanning process always has a certain influence on the sample. Sometimes it is deliberately used to inflict an ordering process^[43] or to manipulate individual molecules.^[14,44] By using a low-current STM with currents below 10 pA, we hoped that this influence could be minimised. The following two clues allow us to exclude the STM as a possible trigger. Firstly, immediately after the observation of a conversion at a certain position of the graphite sample, a location millimetres away was measured (too far away to be influenced by the previous measurements)—only dimers were observed. If the STM triggered the conversion, one should always observe trimers first, which would then be converted. It is worth emphasising that no actual start of the conversion was ever observed inside the imaging window; it always started outside of the measured range and spread to areas much larger than the observed window. This was directly observed when the scan range was enlarged after the observation of the conversion. Secondly a sample of **4** that was annealed for half an hour at 70°C showed only dimers (Figure 10).

We believe that the trimer–dimer interconversion is thermal in origin. Every sample is slightly cooled by the evaporation of the solvent, and then heated to about $30\text{--}40^\circ\text{C}$ in the STM by the measurement. The images showed very little drift at the time of the trimer–dimer conversion, which indicates that a constant temperature had been attained over the sample and microscope. Usually, we observed only one or two domains over a $500\text{ nm} \times 500\text{ nm}$ area. In contrast, a thermally annealed sample showed dimeric structures in many small domains. These observations are consistent with the conversion having a relatively high activation energy that results in only a few initiation events at ambient ($30\text{--}40^\circ\text{C}$) temperatures.

In contrast to other studies,^[23] the observed patterns did not change depending on the measurement technique. The images at the solid–liquid interface (tunnelling while the tip is immersed in a droplet of a solution near saturation lying on a graphite sample) look very similar to those of monolayers prepared by evaporation techniques. Which technique delivers the best resolution in the end seems to depend more on the skills and experience of the operator than the technique. However, no conversion was observed at the liquid–solid interface. An image of **3** at the solid–liquid interface is shown in Figure 11.

In these measurements, only single domains of trimers were observed, and these were error-free. No domain mismatches, no rows of dimers, no vacancies or other irregularities were seen. This indicates that the irregularities of the monolayer, or even impurities, might trigger the conversion.

The suggestion that inverse micelles formed in solutions of *n*-hexane are imprinted directly in two-dimensional analogues on the graphite could be disproved. Measurements from aprotic and protic, polar and apolar solutions show the same metastable trimeric domains, which are converted into a dimeric domain after a delay. All tested solvents (*n*-pentane, *n*-hexane, *n*-decane, toluene, dichloromethane, ace-

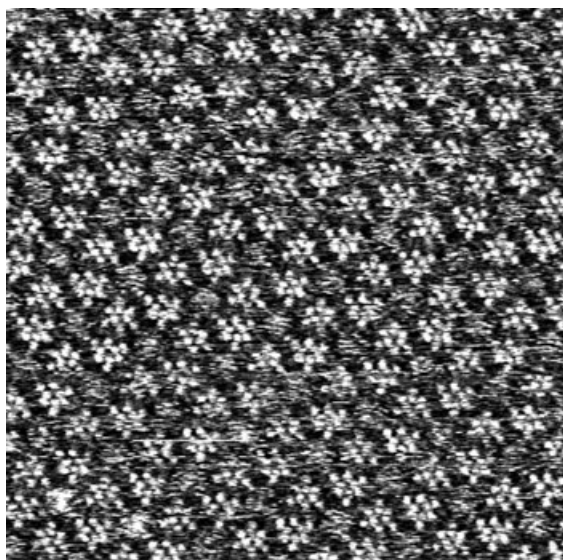


Figure 11. A 40×40 nm image of compound **3** at the solid–liquid interface, measured in a 1-phenyloctane solution. Scanning frequency 5 Hz, $I_t = 8$ pA, $U_{\text{bias}} = -700$ mV.

tone, and 1:1 dichloromethane/methanol) initially showed only trimers with embedded rows of dimers. No influence of the solvent on the formation of trimers or dimers was observed.

In three-dimensional crystallography, it is well known that metastable crystals can be formed, which are then converted into a more stable form.^[45]

Intuitively, a loss of entropy accompanies the observed conversion of trimer to dimer owing to the localisation of the seventh molecule. Clearly for the spontaneous conversion of the trimers to the dimers, the global Gibbs energy change must be negative. It follows that the decrease in entropy must be compensated for by a negative enthalpy change associated with the rearrangement—whether this predominantly arises from the intermolecular or the molecule–substrate interactions is unclear. In the spontaneous conversion, the racemic conglomerate of small trimer domains generates large dimer domains, each of a single chirality.

Conclusion

Octyl-decorated Fréchet dendritic wedges are a powerful recognition motif for the assembly of monolayers on graphite. Herein, we have shown that first generation alcohol **3** and aldehyde **4** both spontaneously form highly structured monolayers upon evaporation of dilute solutions. The aromatic portions of these monolayers may be directly observed by using STM techniques and molecular and submolecular resolution images obtained at room temperature in air. The combination of strong interdigitation interactions between octyl chains of adjacent molecules, of interactions between methylene groups and the graphite surface, and

stacking interactions of the aromatic rings with the graphite result in a very strong binding. Taken in combination with previous studies,^[22,23,42] we propose the use of these residues as a general visualisation marker for the functionalisation of molecular fragments for visualisation in STM.

The specificity of these binding interactions results in the formation of monolayers, which allow us to directly observe a range of phenomena (self-assembly, phase transformation, molecular motion) that have not previously been observed within one molecular system. Specifically, we have observed the initial formation of a metastable monolayer based upon trimeric units, which spontaneously and irreversibly transforms into a monolayer composed of dimeric subunits.

The images obtained are so well resolved that it is possible to unambiguously assign the conformation within individual molecules and describe the supramolecular ordering of molecules into trimeric and dimeric structures and their subsequent assembly into higher-order superstructures. We have explicitly observed the formation of chiral monolayers as a result of the graphite surface binding on only one face of the prochiral monolayers.

We are currently synthesising and studying a variety of other dendron-functionalised structures to establish the generality of this approach.

Experimental Section

General: Commercially available chemicals were reagent grade and were used without further purification. Alcohol **1** was synthesised as described in the literature.^[32] ¹H and ¹³C NMR spectra were recorded on a Bruker DRX500 spectrometer; δ is relative to TMS, referenced to residual CHCl₃. Infrared spectra were recorded on a Shimadzu FTIR-8400S spectrophotometer on neat samples, using a Golden Gate ATR. MALDI-TOF mass spectra were recorded on a Vestec Voyager Elite without matrix. The microanalyses were performed with a Leco CHN-900 instrument.

Compound 3: Methanesulfonyl chloride (1.04 mL, 13.5 mmol) was added over 15 min to a mixture of **1** (1.23 g, 3.38 mmol) and NEt₃ (2.08 mL, 16.9 mmol) in dry CH₂Cl₂ (20 mL) at –15 °C under N₂. After stirring for 1 h at –15 °C, the reaction mixture was poured into a mixture of crushed ice (100 g) and concentrated HCl (10 mL). The CH₂Cl₂ layer was separated, washed with saturated NaHCO₃ solution, dried (Na₂SO₄), and evaporated to give **2** (1.80 g, ca. 80% pure by ¹H NMR spectroscopy, 3.20 mmol) as an oil. Crude **2** (1.33 g, ca. 80% pure, 75.0 μ mol), 3,5-dihydroxybenzyl alcohol (210 mg, 1.50 mmol), K₂CO₃ (840 mg, 6.00 mmol), and [18]crown-6 (15.8 mg, 60.0 μ mol) were stirred vigorously in acetone (30 mL) at 60 °C for 48 h. The solvent was evaporated, water (20 mL) was added, and the mixture extracted three times with dichloromethane (20 mL). The combined organic layers were dried (Na₂SO₄) and evaporated. Chromatography on silica (ethyl acetate/hexane 1:7) yielded **3** as an off-white powder (950 mg, 1.14 mmol, 76%). ¹H NMR spectroscopic and MS data were identical to those previously reported.^[32]

Compound 4: A solution of **3** (64 mg, 76.8 μ mol) in dichloromethane (2 mL) was added to a dry mixture of pyridinium chlorochromate (PCC) (16.7 mg, 77.0 μ mol) and molecular sieves (3) Å, 0.4 g) in dichloromethane (6 mL). The reaction mixture was then allowed to stir at room temperature for 4 h, filtered through Celite, and the solvent evaporated. Chromatography on silica (ethyl acetate/hexane 1:8) yielded **4** as a white powder (58 mg, 69.8 μ mol, 91%). ¹H NMR (500 MHz, CDCl₃, 23 °C): $\delta = 9.89$ (s, 1H; CHO), 7.09 (d, ³J = 2.3 Hz, 2H; H^{2A}), 6.85 (t, ³J = 2.3 Hz, 1H; H^{4A}), 6.55 (d, ³J = 2.2 Hz, 4H; H^{2B}), 6.41 (t, ³J = 2.2 Hz,

2H; H^{dB}), 5.00 (s, 4H; H^{OCH₂B}), 3.94 (t, ³J = 6.6 Hz, 8H; H^{OCH₂CH₂}), 1.77 (tt, ³J = 7.1, 6.7 Hz, 8H; H^{OCH₂CH₂}), 1.44 (tt, ³J = 7.3 Hz, 8H; H^{OCH₂CH₂CH₂}), 1.25–1.37 (m, 32H; H^{(CH₂)₃}), 0.88 ppm (t, ³J = 7.0 Hz, 12H; H^(CH₃)); ¹³C NMR (125 MHz, CDCl₃, 25 °C): δ = 192.01, 160.72, 160.50, 138.51, 138.48, 108.84, 108.42, 105.86, 101.05, 70.54, 68.25, 31.97, 29.51, 29.39, 29.39, 26.20, 22.81, 14.26 ppm; IR (neat): $\tilde{\nu}$ = 2924 s, 2854 m, 1705 m, 1597 s, 1458 m, 1165 s, 1057 m, 833 cm⁻¹ w; MS (MALDI-TOF): m/z: 869.7 [M+K]⁺, 853.7 [M+Na]⁺; elemental analysis calcd (%) for C₅₃H₈₂O₇: C 76.58, H 9.94, N 0.0; found: C 76.23, H 9.86, N 0.0.

X-ray crystal structure analysis of C₅₃H₈₂O₇, 3: Determination of the cell parameters and collection of the reflection intensities were performed on an Enraf-Nonius Kappa CCD diffractometer (graphite monochromated MoK_α radiation, λ = 0.71073 Å). Colourless plate, 0.10 × 0.10 × 0.12 mm, triclinic, space group P $\bar{1}$, a = 10.3990(2), b = 15.6630(3), c = 16.3371(4) Å, α = 100.6870(9), β = 103.4880(10), γ = 101.3648(10)°, T = 123 K, V = 2460.98(9) Å³, Z = 2, μ_{calcd} = 1.124 g cm⁻³, μ = 0.072 mm⁻¹, F(000) = 916. Number of reflections measured 26534 (unique 13990); 5703 observed reflections (I > 3σ(I)), which were used for the determination (direct methods, Denzo/Scapecak,^[46] SIR92^[47]). CRYSTALS^[48] was used for structure refinement. The refinement converged at R = 0.1285 (all data), 0.0485 (observed I > 3σ(I)), wR = 0.1289 (all data), 0.0565 (observed I > 3σ(I)), min and max residual electron density 0.41 and -0.26 e Å⁻³. CCDC -251173 contains the supplementary crystallographic data for this paper. These data can be obtained free of charge from The Cambridge Crystallographic Data Centre via www.ccdc.cam.ac.uk/data_request/cif.

Preparation of monolayers: The monolayers were prepared by solution casting. A small droplet of a dilute solution (about 0.2 mm) was placed onto a freshly cleaved piece of HOPG. After the evaporation of the solvent, the sample was ready for measurements. Perpendicular to the “coffee cup rings” left on the surface by the gradual evaporation of the solvent, a gradient of concentration was found; with any given sample, various concentrations of molecules per surface area could be measured.

STM: A commercial Nanoscope III equipped with a low-current converter was used in all measurements. Mechanically cut Pt-Ir wire was used for tips. The piezo scanner was carefully calibrated with Si-grids and HOPG atoms (for the X and Y axes) and with atomic gold steps (for the Z axes). Nevertheless, the apparent height in STM images is not a height of the molecule but a relative value, describing rather the relative conductivity/tunnelling of the molecules versus the surrounding medium. Some molecules can be imaged with *negative* height.^[49] The measurements presented in this paper were all recorded with the following parameters (exceptions are noted in the figure captions). U_{bias} = -600–700 mV, I_t = 6–20 pA, the scanning frequency was 1 Hz. All images were flattened, but no other image filtering or manipulation was employed, unless noted in the Figure caption. Errors caused by thermal drift of the apparatus could be excluded by carefully checking follow-up scans of the opposite slow scanning direction.

Averaging procedure: To reduce the interaction of the tip with the observed sample, very low tunnelling currents were needed. This resulted in a higher noise level. One possible way to reduce the noise is by using an averaging procedure. We used a procedure programmed for the SXM-shell (University of Basel),^[50] that cuts subimages and calculates an averaged image of these. It is crucial, that these averaging procedures are applied with care; for example, it is easily possible to reduce the apparent symmetry of the trimeric pattern to a threefold symmetry.

The three-dimensional vector representations of the measurements were made with POV-Ray for Windows v.3.5 (www.povray.org).

Quantification of two-dimensional structural motifs: In contrast to three-dimensional crystal structures, the number of possible arrangements in two dimensions is relatively small.^[51] In total, there are 17 plane (space) groups and it is convenient to quantify the structure of the monolayers in crystallographic terms. The trimeric arrangements of both **3** and **4** have identical parameters and are in plane group p6 (no. 16) with a = 5.4 nm, Z = 7. The dimeric arrangements of **3** and **4** are also identical and correspond to plane group p2 (no. 2), a = 2.6; b = 3.1 nm; α = 58°; Z = 2.

Acknowledgements

We thank the Swiss National Science Foundation for financial support through the NRP47 program ‘Supramolecular Functional Materials’ as well as the Universities of Basel and Munich. B. A. H. acknowledges fruitful discussions with Roland Netz.

- [1] *Comprehensive Supramolecular Chemistry, Vol. 9* (Eds.: J. M. Lane, J. L. Atwood, J. E. D. Davies, D. D. MacNicol, F. Vögtle), Pergamon, Oxford, **1996**.
- [2] G. F. Swiegers, T. J. Malefetse, *Chem. Rev.* **2000**, *100*, 3483–3538.
- [3] *Micelles, Microemulsions and Monolayers* (Ed.: D. O. Shah), Science and Technology, M. Dekker, New York, **1998**.
- [4] G. Schmid, *Adv. Eng. Mater.* **2001**, *3*, 737–743.
- [5] G. Schmid, B. Corain, *Eur. J. Inorg. Chem.* **2003**, 3081–3098.
- [6] <http://pubs.acs.org/cen/nanotechnology/7842/7842research.html>.
- [7] V. Balzani, A. Credi, M. Venturi, *ChemPhysChem* **2003**, *4*, 49–59.
- [8] J.-M. Lehn, *Supramolecular Chemistry: Concepts and Perspectives*, VCH, Weinheim, **1995**.
- [9] F. Rosei, M. Schunack, Y. Naitoh, P. Jiang, A. Gourdon, E. Laegsgaard, I. Stensgaard, C. Joachim, F. Besenbacher, *Prog. Surf. Sci.* **2003**, *71*, 95–146.
- [10] S. Chiang, *Chem. Rev.* **1997**, *97*, 1083–1096.
- [11] D. M. Eigler, E. K. Schweizer, *Nature* **1990**, *344*, 524–526.
- [12] G. Meyer, B. Neu, K.-H. Rieder, *Appl. Phys. A* **1995**, *60*, 343–345.
- [13] S.-W. Hla, L. Bartels, G. Meyer, K.-H. Rieder, *Phys. Rev. Lett.* **2000**, *85*, 2777–2780.
- [14] K. Kim, K. E. Plass, A. J. Matzger, *Langmuir* **2003**, *19*, 7149–7152.
- [15] C.-J. Li, Q.-D. Zeng, Y.-H. Liu, L.-J. Wan, C. Wang, C.-R. Wang, C.-L. Bai, *ChemPhysChem* **2003**, *4*, 857–859.
- [16] A. Troisi, M. A. Ratner, *Nano Lett.* **2004**, *4*, 591–595.
- [17] T. A. Jung, R. R. Schlittler, J. K. Gimzewski, *Nature* **1997**, *386*, 696–698.
- [18] A. Stabel, R. Heinz, F. C. De Schryver, J. P. Rabe, *J. Phys. Chem.* **1995**, *99*, 505–507.
- [19] S.-B. Lei, L.-J. Wan, C. Wang, C.-L. Bai, *Adv. Mater.* **2004**, *16*, 828–831.
- [20] F. Moresco, G. Meyer, K.-H. Rieder, H. Tang, A. Gourdon, C. Joachim, *Phys. Rev. Lett.* **2001**, *86*, 672–675.
- [21] J. K. Spong, H. A. Mizes, L. J. J. LaComb, M. M. Dovek, J. E. Frommer, J. S. Foster, *Nature* **1989**, *338*, 137–139.
- [22] E. C. Constable, B. A. Hermann, C. E. Housecroft, L. Merz, L. J. Scherer, *Chem. Commun.* **2004**, 928–929.
- [23] I. Widmer, U. Hubler, M. Stöhr, L. Merz, H.-J. Güntherodt, B. A. Hermann, P. Samorí, J. P. Rabe, P. B. Rheiner, G. Greiveldinger, P. Murer, *Helv. Chim. Acta* **2002**, *85*, 4255–4263.
- [24] S. De Feyter, A. Gesquière, M. M. Abdel-Mottaleb, P. C. M. Grim, F. C. De Schryver, *Acc. Chem. Res.* **2000**, *33*, 520–531.
- [25] X. Qiu, C. Wang, Q. Zeng, B. Xu, S. Yin, H. Wang, S. Xu, C. Bai, *J. Am. Chem. Soc.* **2000**, *122*, 5550–5556.
- [26] G. P. Lopinski, D. J. Moffatt, D. D. M. Wayner, R. A. Wolkow, *Nature* **1998**, *392*, 909–911.
- [27] H. Fang, L. C. Giancarlo, G. W. Flynn, *J. Phys. Chem. B* **1999**, *103*, 5712–5715.
- [28] D. G. Yablon, L. C. Giancarlo, G. W. Flynn, *J. Phys. Chem. B* **2000**, *104*, 7627–7635.
- [29] T. Zambelli, H. Tang, J. Lagoute, S. Gauthier, A. Gourdon, C. Joachim, *Chem. Phys. Lett.* **2001**, *348*, 1–6.
- [30] S. De Feyter, F. C. De Schryver, *Chem. Soc. Rev.* **2003**, *32*, 139–150.
- [31] W. Ho, *J. Chem. Phys.* **2002**, *117*, 11033–11061.
- [32] P. B. Rheiner, D. Seebach, *Chem. Eur. J.* **1999**, *5*, 3221–3236.
- [33] A. Miura, Z. Chen, H. Uji-i, S. De Feyter, M. Zdanowska, P. Jonkheijm, A. P. H. J. Schenning, E. W. Meijer, F. Würthner, F. C. De Schryver, *J. Am. Chem. Soc.* **2003**, *125*, 14968–14969.
- [34] S. De Feyter, M. M. S. Abdel-Mottaleb, N. Schuurmans, B. J. V. Verkuijl, J. H. van Esch, B. L. Feringa, F. C. De Schryver, *Chem. Eur. J.* **2004**, *10*, 1124–1132.

- [35] E. C. Constable, B. A. Hermann, C. E. Housecroft, M. Neuburger and L. J. Scherer, *Chem. Commun.* to be submitted.
- [36] W. Mamdouh, H. Uji-I, A. E. Dulcey, V. Percec, S. De Feyter, F. C. De Schryver, *Langmuir* **2004**, *20*, 7678–7685.
- [37] P. Wu, Q. Fan, G. Deng, Q. Zeng, C. Wang, C. Bai, *Langmuir* **2002**, *18*, 4342–4344.
- [38] A. J. Fisher, P. E. Blöchl, *Phys. Rev. Lett.* **1993**, *70*, 3263–3266.
- [39] a) C. B. France, B. A. Parkinson, *J. Am. Chem. Soc.* **2003**, *125*, 12712–12713; b) M. Böhringer, K. Morgenstern, W.-D. Schneider, R. Berndt, F. Mauri, A. De Vita, R. Car, *Phys. Rev. Lett.* **1999**, *83*, 324–327; c) J. Weckesser, A. De Vita, J. V. Barth, C. Cai, K. Kern, *Phys. Rev. Lett.* **2001**, *87*, 096101/1–096101/4; d) L. Pérez-García, D. B. Amabilino, *Chem. Soc. Rev.* **2002**, *31*, 342–356; e) S. De Feyter, A. Gesquière, K. Wurst, D. B. Amabilino, J. Veciana, F. C. De Schryver, *Angew. Chem.* **2001**, *113*, 3317–3320; *Angew. Chem. Int. Ed.* **2001**, *40*, 3217–3220; f) M. Böhringer, K. Morgenstern, W.-D. Schneider, R. Berndt, *Angew. Chem.* **1999**, *111*, 832–834; *Angew. Chem. Int. Ed.* **1999**, *38*, 821–823; g) J. V. Barth, J. Weckesser, G. Trimarchi, M. Vladimirova, A. De Vita, C. Cai, H. Brune, P. Günter, K. Kern, *J. Am. Chem. Soc.* **2002**, *124*, 7991–8000; h) L. C. Giancarlo, G. W. Flynn, *Acc. Chem. Res.* **2000**, *33*, 491–501.
- [40] The graphite atoms cannot be resolved by the scanning parameters used to image the adsorbed molecules.
- [41] F. H. Herbstein in *Comprehensive Supramolecular Chemistry*, Vol. 6, (Eds.: J. L. Atwood, J. E. D. Davies, D. D. MacNicol, F. Vögtle, F. Toda, R. Bishop), Pergamon, Oxford, **1996**, pp. 61–84.
- [42] L. J. Scherer, L. Merz, E. C. Constable, C. E. Housecroft, M. Neuburger, B. A. Hermann, *J. Am. Chem. Soc.* **2005**, in press.
- [43] J.-R. Gong, S.-B. Lei, L.-J. Wan, G.-J. Deng, Q.-H. Fan, C.-L. Bai, *Chem. Mater.* **2003**, *15*, 3098–3104.
- [44] A. J. Heinrich, C. P. Lutz, J. A. Gupta, D. M. Eigler, *Science* **2002**, *298*, 1381–1387.
- [45] W. Ostwald, *Z. Phys. Chem. (Leipzig)* **1897**, *22*, 289–330.
- [46] Z. Otwinowski, W. Minor, *Methods Enzymol.* **1997**, *276*, 307–326.
- [47] A. Altomare, G. Casciaro, G. Giacovazzo, A. Guagliardi, M. C. Burla, G. Polidori, M. Camalli, *J. Appl. Crystallogr.* **1994**, *27*, 435.
- [48] P. W. Betteridge, J. R. Carruthers, R. I. Cooper, K. Prout, D. J. Watkin, *J. Appl. Crystallogr.* **2003**, *36*, 1487.
- [49] C. Klink, L. Olesen, F. Besenbacher, I. Stensgaard, E. Laegsgaard, N. D. Lang, *Phys. Rev. Lett.* **1993**, *71*, 4350–4353.
- [50] D. Brodbeck, D. Buerger, R. Hofer, G. Tarrach, University of Basel, 1993–2004.
- [51] *International Tables for Crystallography, Vol A* (Ed.: T. Hahn), Kluwer, Dordrecht, **2002**.

Received: September 27, 2004
Published online: February 4, 2005